Mon. Not. R. astr. Soc. (1981) 194, 301–330

Observations of compact radio sources with the 5-km telescope

R. A. Laing* *Mullard Radio Astronomy Observatory, Cavendish Laboratory, Madingley Road, Cambridge CB3 0HE*

Received 1980 June 13; in original form 1980 March 24

Summary. Twenty-five small-diameter radio sources have been observed at 15.4 GHz with the Cambridge 5-km telescope. A method which uses an unresolved component in the field of view as a phase reference has been developed in order to search for faint outer structure around bright compact objects. Maps are presented for 11 of the sources. It is suggested that all sources selected in low-frequency surveys have outer structure on scales > 0.5 arcsec.

1 Introduction

This paper describes observations of 25 compact extragalactic radio sources made with the Cambridge 5-km telescope at 15.4 GHz, together with a few observations at 5.0 and 2.7 GHz. The objectives of this study are as follows:

(1) The determination of the structures of sources which were unresolved or barely resolved in previous observations with the 5-km telescope at 5.0 GHz (Jenkins, Pooley & Riley 1977 and references therein).

(2) A search for outer structure around compact radio sources, using the central components as phase references in order to improve the dynamic range of the maps. This investigation was prompted by:

(a) The mapping of extended structure in 3C 345, 371, 418 and 454.3 by Davis, Stannard & Conway (1977) and by Perley & Johnston (1979).

(b) The suggestion by Duffett-Smith (1980) that very few sources detected in a survey of interplanetary scintillation at 81.5 MHz (Readhead & Hewish 1974) are < 0.4 arcsec in overall extent.

(c) The realization that compact sources selected at low frequencies (e.g. 178 MHz in the 3C survey) must have appreciable structure on a scale of 0.2–1.0 arcsec because the very compact components seen at higher frequencies will be self-absorbed. At 15.4 GHz, the flux density of a 3C source will be at least 0.1 Jy if the spectral index $\alpha = 1$ ($S \propto \nu^{-\alpha}$). Given a

* Present address: National Radio Astronomy Observatory, Edgemont Road, Charlottesville, Virginia 22901, USA.

dynamic range of between 10 and 20:1 (which can usually be attained by phase-referencing; see Section 3.2), it should be possible to detect such structure close to a source with $S \sim 1-2$ Jy at 15.4 GHz.

The observations are described in Section 2. The effects of atmospheric phase errors on aperture synthesis observations are outlined in Section 3.1 and a technique for their suppression is presented in Section 3.2. Some limitations of the method are exposed by tests on artificial sources in Section 3.3. The results are presented as tables of component parameters and as contour maps in Section 4; notes on individual sources are given in Section 5, and Section 6 contains a brief discussion.

Sources whose emission at high frequencies is dominated by a central component (CC) will be referred to as *core* sources in order to distinguish them from objects with two components, one on either side of the identification, but with no CC.

2 Observations

Observations were made with the 5-km telescope at 15.375 GHz using 16 interferometer spacings with a maximum baseline of 4.5744 km. At this frequency, the synthesized beam area (FWHM) is 0.67×0.67 cosec δ arcsec^2 if a Gaussian grading to 30 per cent at the maximum baseline is used. Some of the maps in this paper have been made with a uniform grading of the aperture; the resolution is then improved (FWHM = 0.58×0.58 cosec δ arcsec^2) at the expense of a higher sidelobe level. The first grating response is an ellipse with axes of 14×14 cosec δ arcsec^2 and is much larger than any of the structure discussed here. Parallel feeds in pa 0 or 90° were used, measuring the Stokes parameters $I+Q$ and $I-Q$ respectively. Note that the derived brightness distributions differ appreciably from those of total intensity, I, if the source is highly polarized. The flux-density scale was based on a value of $I = 3.38$ Jy for 3C 286 (derived from Genzel *et al.* 1976 with a small correction for the frequency difference) and this source was assumed to be 11.1 per cent polarized in pa 32°.5 (Tabara & Inoue 1980).

The sources are listed in Table 1, which contains the following information:

Columns 1 and 2: The IAU and common names of the source.

Column 3: Whether or not the source has significant resolved structure. An asterisk in this

Table 1. Observations at 15.4 GHz.

(a) Sources for which the phase-referencing technique of Sec. 3.2 has been used.

IAU name	Common	Date of observation day/month/year	Stokes parameter	Sampling interval /min
0127 + 234	3C 43	4/1/76	I+Q	5
		26/1/77	I-Q	5
0134 + 329	3C 48	9/1/76	I+Q	5
		14/1/76	I+Q	5
		24/3/76	I+Q	1
		1/12/76	I-Q	5
		1/1/77	I-Q	5
0138 + 136	3C 49	6/3/77	I-Q	5
0345 + 337	3C 93.1	16/1/76	I+Q	1
0518 + 165	3C 138	20/12/75	I+Q	5

Table 1 – *continued*

IAU name	Common	Date of observation day/month/year	Stokes parameter	Sampling interval /min
		11/1/76	I+Q	5
		21/1/76	I+Q	1
0538 + 498	3C 147	13/11/76	I-Q	5
		30/11/76	I-Q	5
		29/12/76	I-Q	5
0831 + 557	4C 55.16	21/12/75	I+Q	5
		9/4/76	I+Q	5
		16/1/77	I-Q	5
0851 + 202	OJ 287	2/12/76	I-Q	5
		15/12/76	I-Q	5
		31/12/76	I-Q	5
		9/1/77	I-Q	5
		15/1/77	I-Q	5
1040 + 123	3C 245*	5/3/77	I-Q	5
1328 + 307	3C 286	30/12/75	I+Q	5
		31/3/76	I+Q	5
		5/1/77	I-Q	5
1419 + 420	3C 299*	2/4/77	I-Q	5
1458 + 718	3C 309.1*	21/11/76	I-Q	5
		28/11/76	I-Q	5
		30/11/76	I-Q	5
1828 + 487	3C 380*	28/12/75	I+Q	5
2005 + 403	-	18/1/76	I+Q	5
2037 + 511	3C 418*	26/3/77	I-Q	5
2230 + 114	CTA 102	10/11/76	I-Q	5
2249 + 185	3C 454	12/2/77	I-Q	1
(b) Sources for which phase-referencing has not been used				
0758 + 144	3C 190*	17/2/77	I-Q	1
0802 + 104	3C 191*	19/2/77	I-Q	1
1003 + 351	3C 236*	16/4/76	I+Q	5
1019 + 222	3C 241	11/2/77	I-Q	1
		14/2/77	I-Q	1
1203 + 645	3C 268.3*	5/5/75	I+Q	5
1443 + 773	3C 303.1	10/1/76	I+Q	5
		8/2/77	I-Q	1
1447 + 771	3C 305.1*	6/3/77	I-Q	1
		15/4/77	I-Q	1
1511 + 263	3C 315*	20/4/77	I-Q	1

column indicates that the source is well-resolved and that a map is presented in one of the Figs 4–15.

Column 4: Date of observation.

Column 5: The Stokes parameters of the observation ($I + Q$ or $I - Q$).

Column 6: The sampling interval. Observations made using an unresolved source outside the field as a phase calibrator, as described by Riley & Pooley (1978), have a sampling interval of 1 min; the remainder of the runs were sampled at 5-min intervals.

The phase-referencing method of Section 3.2 has been used for those sources with bright compact components (Table 1a). The observations of 3C 236 and 315 refer only to the central components coincident with the associated galaxies. In addition, the 5.0-GHz data presented for 3C 245, 299 and 380 by Riley & Pooley (1975) and by Jenkins *et al.* (1977) have been reanalysed and new observations of 3C 380 at 2.7 GHz have been made (see Section 5).

3 Data reduction

3.1 PHASE ERRORS IN HIGH-FREQUENCY SYNTHESIS OBSERVATIONS

Hargrave & Shaw (1978) discussed the effects of large-scale atmospheric irregularities on aperture-synthesis observations with the 5-km telescope at 5.0 GHz; their conclusions may be summarized as follows:

(1) The irregularities occur in a non-dispersive medium (phase change proportional to $1/\lambda$) and must therefore be associated with water-vapour in the troposphere.

(2) For the majority of the irregularities, the phase change is proportional to baseline, which means that the horizontal scale sizes are greater than the length of the telescope.

(3) The scale sizes exceed the scale height of water vapour in the troposphere, so that the magnitude of a phase error increases roughly as sec z (z is the zenith angle).

(4) Characteristic durations vary from ~ 1 min to a few hours.

Such errors set the most important limitation to high-frequency synthesis observations (see Hamaker 1979a for a more detailed review). They can be ascribed principally to linear phase gradients, so that their main effect is to shift the apparent instantaneous position of the source and its associated corrugation (Bracewell & Thompson 1973). If the shift persists for some time, the corrugations are superposed over a range of hour angles and tend to interfere constructively, all negative contributions coinciding on one side of the source position and all positive contributions coinciding on the opposite side. The sidelobes caused by atmospheric phase variations are particularly troublesome if the source has a bright, point-like component. If the phase error varies appreciably over a single sampling interval, then amplitude will be lost. This effect is most pronounced at low elevations, where the phase changes are largest, but is easily recognizable, and badly affected observations have been discarded.

Calibration on an unresolved source near the field of interest (Riley & Pooley 1978) was used for several of the observations, but could only correct for variations on time-scales longer than ~ 30 min, because observations of source and calibrator are not simultaneous. The use of a point source in the field of view as a phase reference (e.g. Peckham 1973) appeared to be the most promising technique for the analysis of the present observations, because the brightness distributions of several of the sources are dominated by unresolved components. Two variants are possible, involving the isolations of the point-source response in the map plane or the aperture plane respectively. The latter alternative is used here; the

method was suggested by J. E. Baldwin and P. J. Warner and is discussed below. Hamaker 1979b) mentions a similar method ('kneading').

3.2 A METHOD FOR THE REMOVAL OF PHASE ERRORS CAUSED BY TROPOSPHERIC IRREGULARITIES

Consider a source whose small-scale structure is dominated by a single unresolved component. The visibility amplitude on the longest baseline of the telescope is then mainly that of the point component, and if a phase shift is applied so that the point source is at the map centre, both the amplitudes and the phases on the long baselines are approximately constant over the observation. A one-dimensional Fourier transform of the visibility amplitudes for a single sample then shows a peak at the origin, superimposed on a smoother background. The reference source is the dominant compact feature in the brightness distribution, so that it is always possible to locate the peak unambiguously. The effect of a phase gradient.

$$\phi = \phi_0(u/d),$$

where u is the baseline, d is the maximum baseline, and ϕ_0 is a constant, is to shift the corresponding corrugation by an amount

$$\Delta = \frac{\phi_0}{2\pi}(\lambda/d).$$

This appears as a uniform shift of the one-dimensional Fourier transform. The position of the peak of the transform can be determined, and if it is assumed that the reference source is at the map centre, then a suitable phase shift can be introduced to realign the associated corrugation. If this procedure is applied to all the samples of the visibility function in turn, the effects of phase irregularities on a time-scale longer than the sampling interval can be removed.

In order to estimate the dynamic range which can be achieved by phase-referencing in the absence of confusing structure (see Section 3.3), maps have been made using the corrected phases for observations of sources which show no evidence for resolution even on the longest baseline of the telescope. Point sources were then subtracted from the map centres to leave residuals (corresponding to deviations from the assumed form of the phase variation and to amplitude errors) whose maximum values were typically 4 per cent and in the best cases could be as low as 2 per cent. At 5.0 GHz, where the phase errors are reduced by a factor ~ 3, a typical value for the maximum residual is 1 per cent. The values of the residuals for 15 observations of unresolved sources are given in Section 4.4 (Table 4).

The present technique is a close analogue of that used by Perley & Johnston (1979) which is itself, if all baselines are correlated, equivalent to the initial step in the hybrid mapping procedure described by Readhead & Wilkinson (1978).

3.3 LIMITATIONS OF THE METHOD

The phase-referencing method is expected to break down when the reference source is not dominant on the longest baselines. To illustrate the possible pitfalls, the procedure has been applied to three model brightness distributions at 15.4 GHz. That of Fig. 1(a) consists of two point sources separated by 5 arcsec, with flux densities in the ratio 5:1, the brighter component has been used as a phase reference. The phase-referenced and difference maps are shown in Fig. 1(b) and (c), respectively. Over a small range of hour angle, the maxima

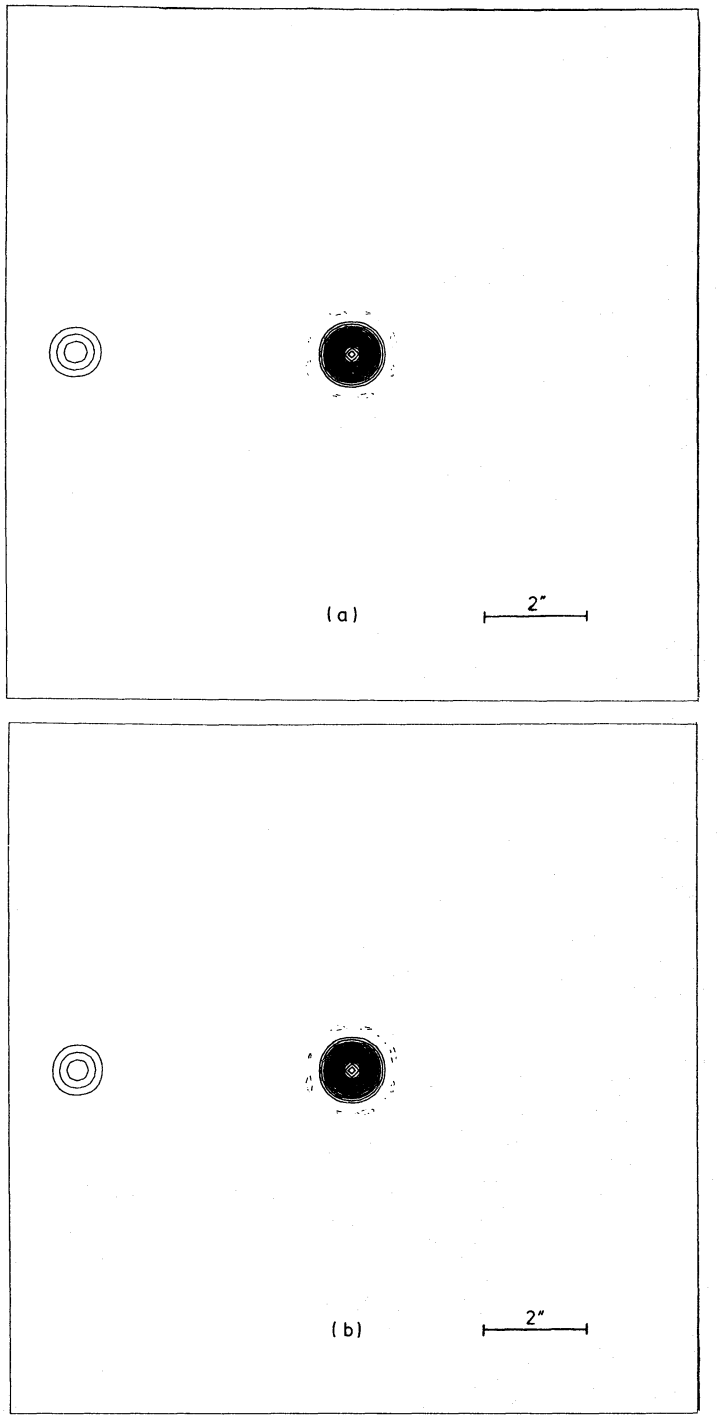

Figure 1. The results of applying the phase-referencing method to a model brightness distribution consisting of two point sources separated by 5 arcsec in pa 90° and with flux densities in the ratio 5 :1. (a) A contour map of the model brightness distribution. There are 20 contours to the peak of the brighter component. (b) A contour map of the brightness distribution after phase-referencing. The contour interval is the same as that in (a). (c) A map of the difference between the brightness distributions before and after phase-referencing. The contour interval is 1/100 of that in (a) and (b).

in the one-dimensional transform which correspond to the two components overlap and the position of the reference peak is determined incorrectly. Such an effect will occur when the corrugations are slightly misaligned with the source axis (east–west in this example). The residual structure therefore corresponds to corrugations which are aligned approximately

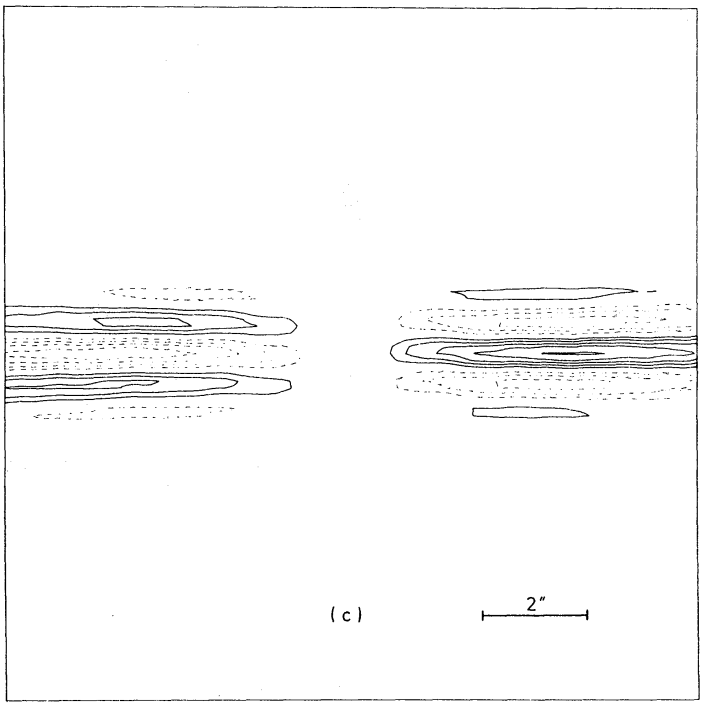

Figure 1 – *continued*

east–west, as can be seen on the difference map of Fig. 1(c). The residuals are localized close to the weaker component of the model and its inversion in the map centre. This is a general feature of the phase-referencing process. The phase errors are small so that the brightness distribution is antisymmetric. The peak of the residual structure is only 1.3 per cent of the flux density of the *weaker* component of the source.

Similar results are obtained for the model of Fig. 2(a), which consists of a point source and a Gaussian component of FWHM = 3 arcsec separated by 5 arcsec. The flux density of the extended component is four times that of the point source and the effects of phase-referencing on the point component are shown in Fig. 2(b) and (c). Despite the fact that the extended component dominates on the shorter baselines, the spurious features are small (~ 3 per cent of the peak brightness of the extended component) and confined to pa 90°.

Serious inaccuracies are introduced, however, if there is structure close to the central source, so that the peak of the transform is determined incorrectly for a substantial range of hour angles. This problem is illustrated in Fig. 3 for a model consisting of two point sources with flux densities in the ratio 10:1 separated by the half-power beamwidth (0.67 arcsec) The error map (Fig. 3c) now has a peak value of ~ 30 per cent of the flux density of the weaker source. If a source is subtracted from the map centre (Fig. 3d), then the residual structure appears double, although the spurious component is not beam-shaped and is associated with two negative features. It is unlikely that this distinction would be apparent in practice, so that sources with structure only on one side of a bright central component may not be distinguishable from those with structure on both sides, if the total extent of such emission is less than a beamwidth. *This is an important limitation, which must be borne in mind for the compact sources discussed later.* The importance of this effect has been evaluated for all the phase-referenced brightness distributions, and maps are not shown for those sources where significant distortions may have been introduced.

Restrictions on the use of the method may be summarized as follows:

(1) The reference source must be dominant on the longest interferometer baselines.

(2) Spurious features occur at particular (predictable) position angles if bright structure

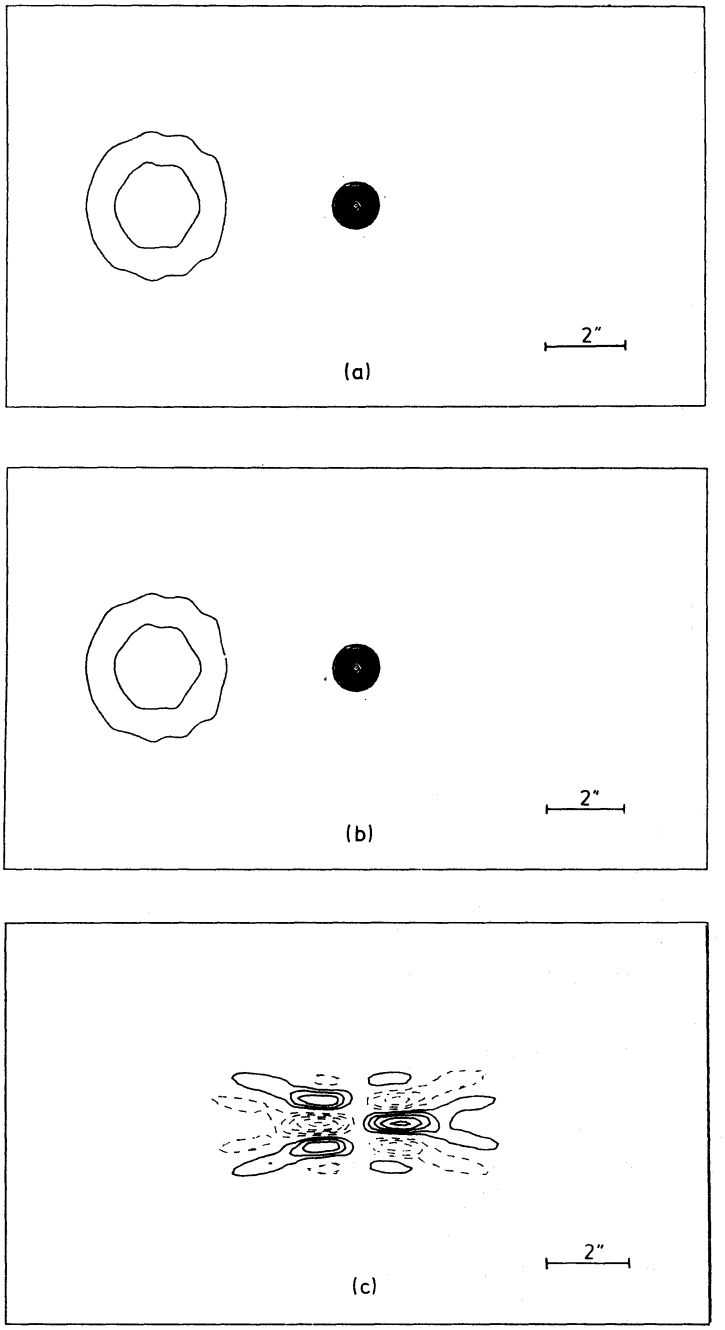

Figure 2. The results of applying the phase-referencing method to a model brightness distribution consisting of a point source and a Gaussian component of FWHM = 3 arcsec, separated by 5 arcsec. The flux density of the extended component is four times that of the point source. (a) A contour map of the model brightness distribution. There are 15 contours to the peak of the point component. (b) A contour map of the brightness distribution after phase-referencing. The contour interval is the same as that in (a). (c) A map of the difference between the brightness distributions before and after phase-referencing. The contour interval is 1/50 of that in (a) and (b).

other than the reference source is present. These are appreciable if such structure is close to the reference source.

(3) Phase deviations must be accurately proportional to spacing. In practice, deviations from proportionality cause small residual errors.

(4) There must be a large enough signal-to-noise ratio for a single sample. This has restricted the use of the method to reference sources with 15.4 GHz flux densities in excess of ~ 0.2 Jy.

(5) The phase must remain approximately constant over a single sample. If this is not true, then the phase-referencing technique breaks down and there is a loss of amplitude. For this reason, observations sampled at 1-min intervals proved to be much better than those sampled at the usual 5-min intervals, provided that condition (4) was still satisfied.

(6) Absolute positional information is lost because the reference source is moved to the assumed map centre.

Despite these restrictions, the method has proved useful for making maps of sources consisting of a single point component together with surrounding weak or extended emission.

4 Results

4.1 OPTICAL DATA

Table 2 lists magnitudes, redshifts, and positions for optical objects associated with the sources discussed in this paper, together with the conversion factors between linear and angular scales ($\Omega_0 = 0$ and $H_0 = 50\,\mathrm{km\,s^{-1}\,Mpc^{-1}}$).

4.2 CONTOUR MAPS

Contour maps of the brightness distributions of the resolved sources are shown in Figs 4–15. 15.4-GHz maps are given for all the sources, together with 5.0-GHz maps of 3C 245 and 299 and a 2.7-GHz map of 3C 380. VLBI maps of the central regions of 3C 236, 286 and 380 are also presented; these are discussed in Section 5. On maps made with the 5-km telescope, an L shape indicates the angular and linear scales and the number following 'CI' gives the contour level in mJy. Contours are plotted at $\pm 1, \pm 2, \ldots$ times the contour interval. The half-power beam is indicated by a shaded ellipse. The Stokes parameters of the 15.4-GHz observations are given in the headings to the maps; 'UG' indicates that the map was made using a uniform grading of the aperture. Details of maps made with other telescopes are given in the figure captions. The reference source has been subtracted in order to show the extended structure in all maps made using phase-referencing except that of 3C 245. Note that positions on a phase-referenced map are measured relative to that assumed for the central source. On maps made without phase-referencing, crosses denote the positions of associated optical objects. (Table 2).

4.3 COMPONENT PARAMETERS

The data for each well-resolved source are presented in Tables 3(a) and (b) for phase-referenced and uncorrected observations respectively as follows:

Column 1: The name of the source.

Column 2 and 3: The coordinates (1950.0) of the components, with estimated errors. An asterisk indicates that the position is an assumed value for a reference source. For the phase-referenced observations of Table 3(a), the positions of the outer components are determined *relative to that of the reference source.*

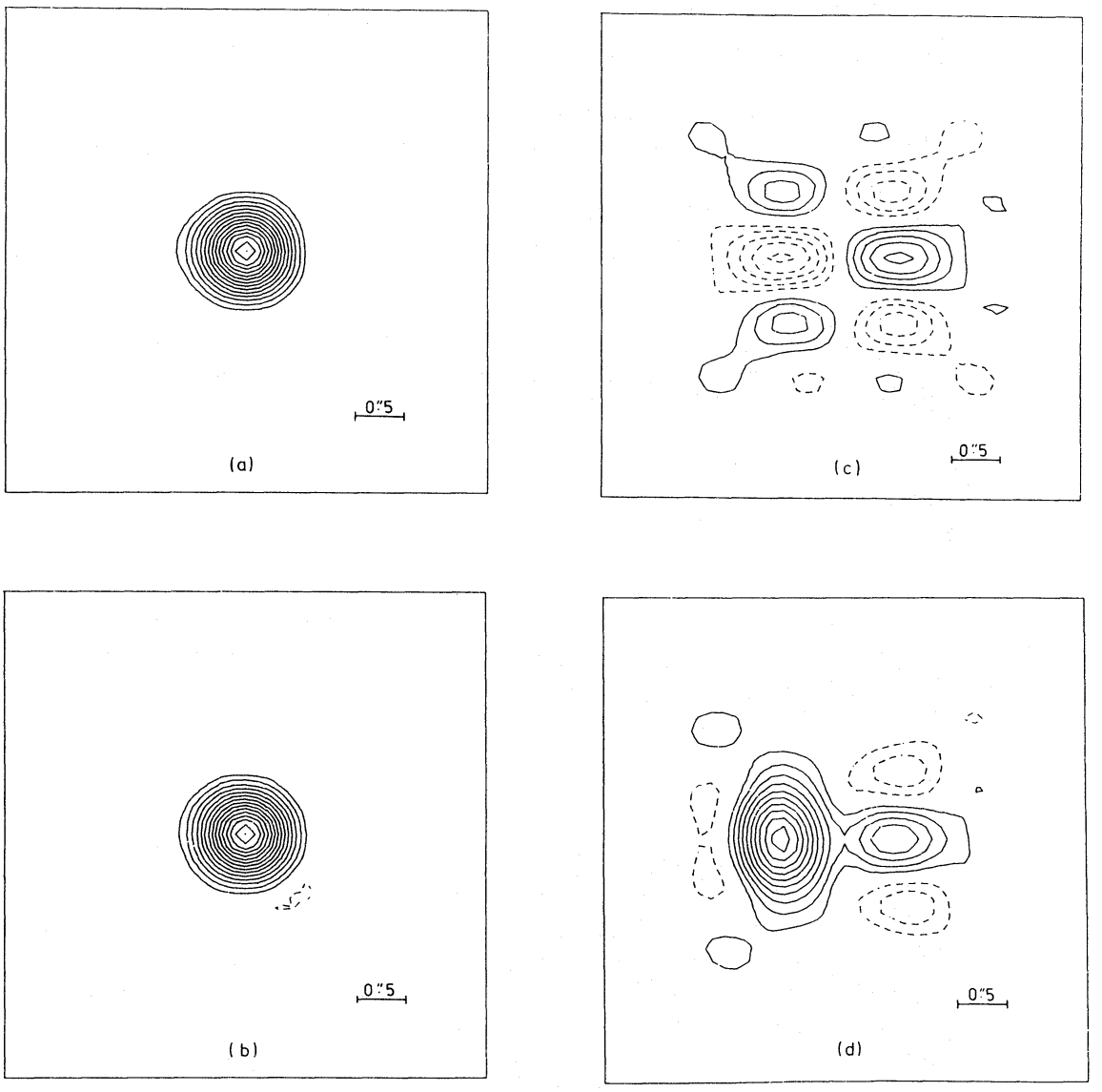

Figure 3. The results of applying the phase-referencing method to a model brightness distribution consisting of two point sources with flux densities in the ratio 10:1 separated by 0.67 arcsec in pa 90° (the weaker component is on the left). (a) A contour map of the model brightness distribution. There are 15 contours to the peak. (b) A contour map of the brightness distribution after phase-referencing with the same contour interval as in (a). (c) A map of the difference between the brightness distributions before and after phase-referencing. The contour interval is 1/25 of that in (a) and (b). (d) A phase-referenced map from which a point source at the map centre has been subtracted. The contour interval is 1/100 of that in (a) and (b).

Columns 4 and 5: The angular extents of each component parallel and perpendicular to its major axis. Gaussian brightness distributions have been assumed; the quoted values are FWHM. Upper limits refer to RA (ω_1) and Dec (ω_2).

Column 6: The flux density of each component at 15.4 GHz, with the estimated error.

Column 7: The total flux density of the source. If resolved structure is present, this will be significantly greater than the sum of the component flux densities. An asterisk denotes a value assumed for calibration purposes.

Column 8: The overall extent of the source.

Column 9: The position angle of the major axis of the source.

Table 2. Optical data.

Source	Identification	Magnitude	Redshift	RA(1950.0) h m s	Dec.(1950.0) o ' "	References Position	References V and z	kpc/ arcsec
3C 43	Quasar	20*	1.459	01 27 15.04 ± 0.05	23 22 51.5 ± 0.7	8	11	12.1
3C 48	Quasar	16.2	0.367	01 34 49.823 ± 0.005	32 54 20.39 ± 0.06	3		6.8
3C 49	Galaxy	21*		01 38 28.41 ± 0.07	13 38 19.9 ± 1.0	12	12	
3C 93.1	Galaxy	19*	0.243	03 45 35.71 ± 0.05	33 44 06.4 ± 0.4	18		5.1
3C 138	Quasar	18.84	0.759	05 18 16.521 ± 0.003	16 35 26.60 ± 0.05	5		9.8
3C 147	Quasar	17.8	0.545	05 38 43.529 ± 0.005	49 49 42.88 ± 0.05	5		8.5
3C 190	Quasar	20*	1.195	07 58 45.00 ± 0.10	14 23 04.5 ± 1.5	17	15	11.5
3C 191	Quasar	18.4	1.955	08 02 03.77 ± 0.06	10 23 57.0 ± 0.8	8		12.9
4C 55.16	Galaxy	17.5	0.242	08 31 04.338 ± 0.018	55 44 41.70 ± 0.16	3		5.1
OJ 287	BL Lac object	12.7 - 15.6		08 51 57.257 ± 0.003	20 17 58.13 ± 0.04	5	9	
3C 236	Galaxy	15.97	0.0989	10 03 05.37 ± 0.03	35 08 48.1 ± 0.4	16		2.5
3C 241	Galaxy	22.6 (r)		10 19 09.44 ± 0.04	22 14 40.7 ± 0.5	7	7	
3C 245	Quasar	17.25	1.029	10 40 05.96 ± 0.05	12 19 15.9 ± 0.7	8		11.0
3C 268.3	Galaxy	20*	0.371	12 03 54.28 ± 0.09	64 30 18.6 ± 0.4	10		6.8
3C 286	Quasar	17.25	0.846	13 28 49.651 ± 0.007	30 45 58.50 ± 0.09	3		10.3
3C 299	Galaxy	19.43	0.367	14 19 06.29 ± 0.10	41 58 30.2 ± 1.0	13		6.8
3C 303.1	Galaxy	19*	0.267	14 43 53.7 ± 0.2	77 20 05.1 ± 0.7	8		5.5
3C 305.1	Galaxy	21*	0.456	14 47 49.0 ± 1.0	77 08 46.0 ± 2.0	10		7.7
3C 309.1	Quasar	16.78	0.904	14 58 56.657 ± 0.014	71 52 11.29 ± 0.06	3		10.5
3C 315	Galaxy	16.8	0.1083	15 11 30.825 ± 0.022	26 18 38.96 ± 0.30	6		2.7
3C 380	Quasar	16.81	0.691	18 28 13.513 ± 0.016	48 42 40.45 ± 0.12	2		9.5
2005+403	Quasar	19.5	1.736	20 05 59.561 ± 0.026	40 21 02.74 ± 0.30	1	4	12.6
3C 418	Quasar	20*	1.686	20 37 07.30 ± 0.10	51 08 35.0 ± 1.0	18	10	12.5
CTA 102	Quasar	17.3	1.037	22 30 07.830 ± 0.006	11 28 22.73 ± 0.09	3	14	11.0
3C 454	Quasar	18.54	1.757	22 49 07.74 ± 0.09	18 32 43.9 ± 1.2	8		12.6

Notes

The magnitudes have been measured photometrically in the *V* band unless otherwise stated. The magnitude of 3C 241 is that in the r (red) band of Wade *et al.* (1979); an asterisk denotes an estimate. Magnitudes and redshifts have been taken from the compilations of Smith, Spinrad & Smith (1976) or Burbidge & Crowne (1979) whenever possible; additional references are as follows:

1 Argue (private communication);
2 Argue & Kenworthy (1972);
3 Argue, Clements, Harvey & Murray (1978);
4 Boksenberg *et al.* (1976);
5 de Vegt & Gehlich (1978);
6 Griffin (1963);
7 Gunn *et al.* (in preparation);
8 Jenkins, Pooley & Riley (1977);
9 Kinman (1976);
10 Kristian, Sandage & Katem (1974);
11 Kristian, Sandage & Katem (1978);
12 Riley, Longair & Gunn (1980);
13 Riley & Pooley (1975);
14 Schmidt (1965);
15 Spinrad (private communication);
16 Wills, Wills & Douglas (1973);
17 Laing *et al.* (1978);
18 Measurements on the prints of the Palomar Sky Survey, relative to stars in the AGK 3 catalogue as described by Riley & Pooley (1975).

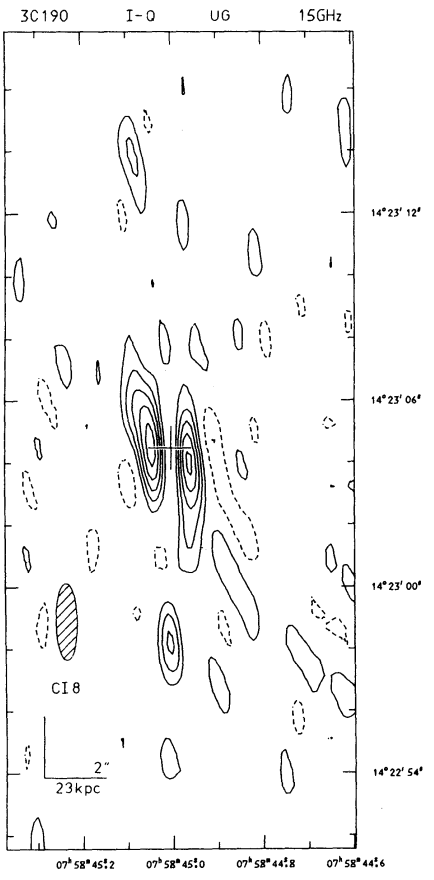

Figure 4

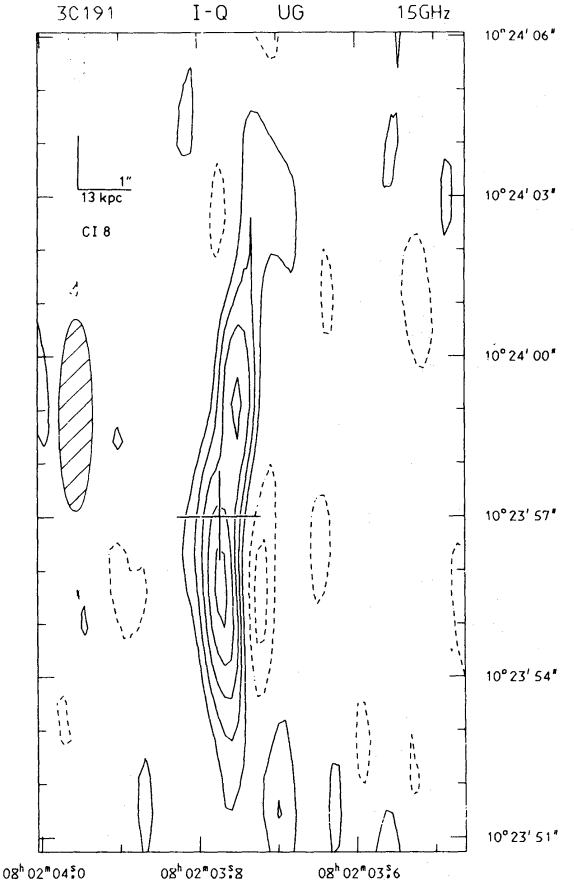

Figure 5

Figure 4. 3C 190 (a map made without phase-referencing using a uniform grading of the aperture).

Figure 5. 3C 191 (a map made without phase-referencing using a uniform grading of the aperture).

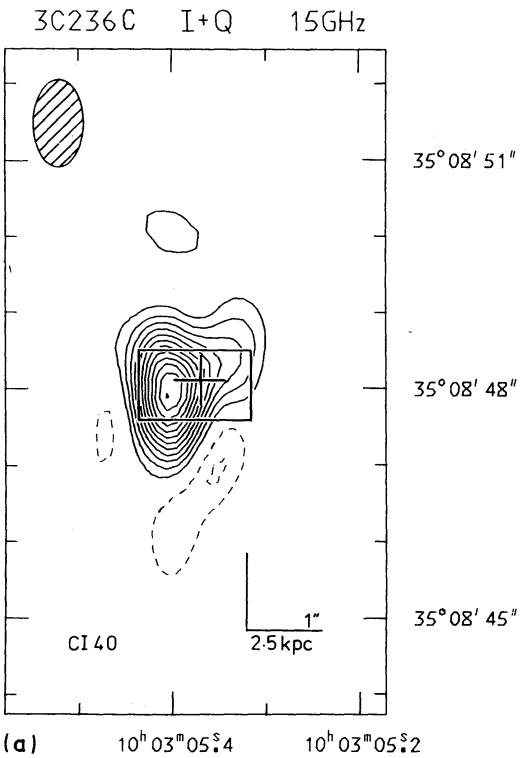

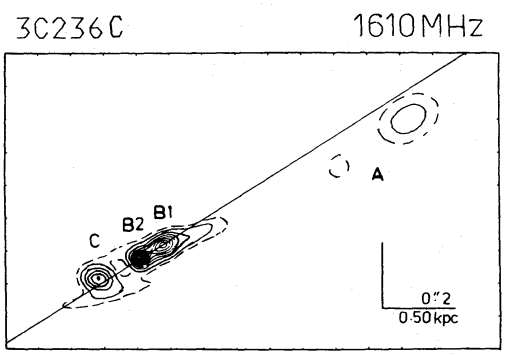

Figure 6. 3C 236. (a) A 15.4-GHz map of the central component (not phase-referenced). The box indicates the area covered by Fig. 13(b). (b) A VLBI model of the central component, from Schilizzi *et al.* (1979). This model was made using three-station observations at 1.6 GHz and has been smoothed with a circular Gaussian beam of FWHM = 0.037 arcsec.

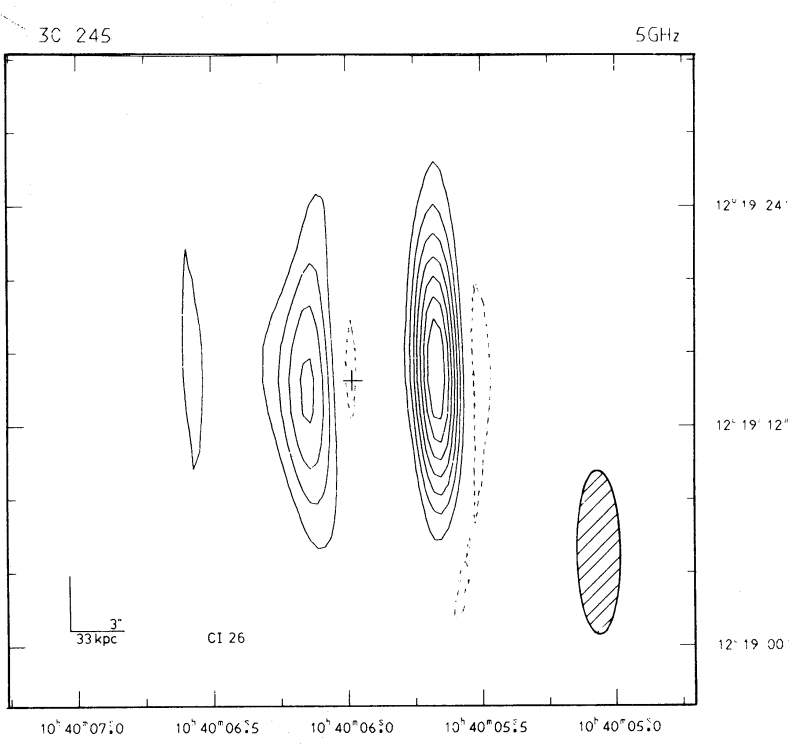

(a)

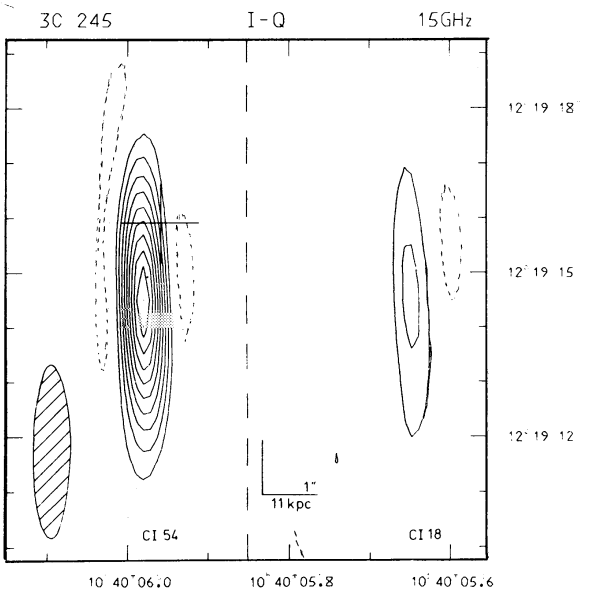

(b)

Figure 7. 3C 245. Both maps are phase-referenced. (a) 5.0 GHz. A point source of 0.91 Jy has been subtracted from the position marked by the cross. The lowest contour is 2.9 per cent of the peak. (b) 15.4 GHz. The reference source has not been subtracted. The cross marks the position of the associated quasar as measured by Jenkins *et al.* (1977). The contour intervals in the two panels of the map differ by a factor of 3.

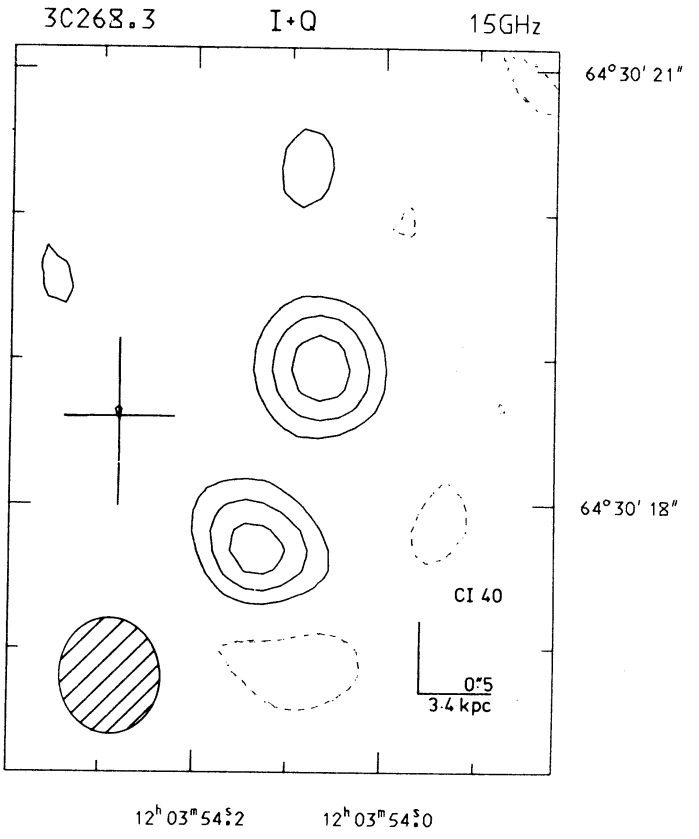

Figure 8. 3C 268.3 (not phase-referenced).

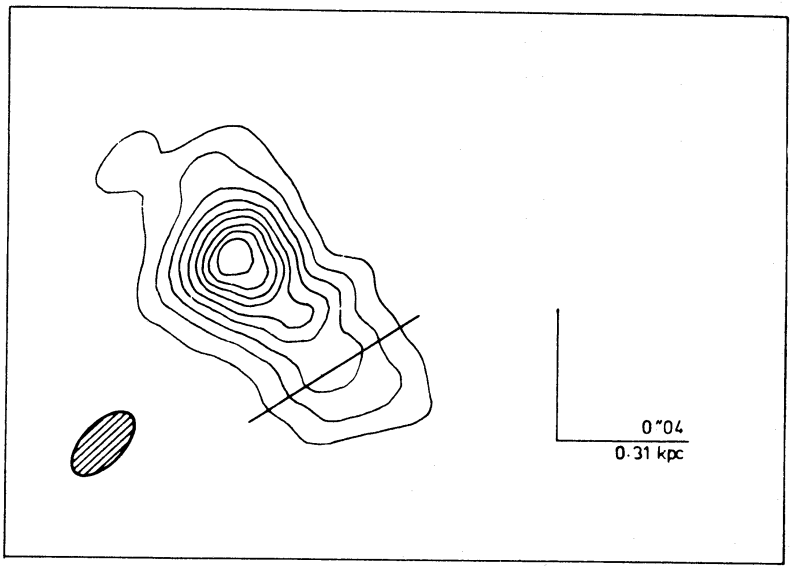

Figure 9. 3C 286. A VLBI map at 609 MHz, from Wilkinson *et al.* (1979). The apparent direction of the magnetic field (corrected to infinite frequency assuming that the radiating region is optically thin) is indicated by the straight line.

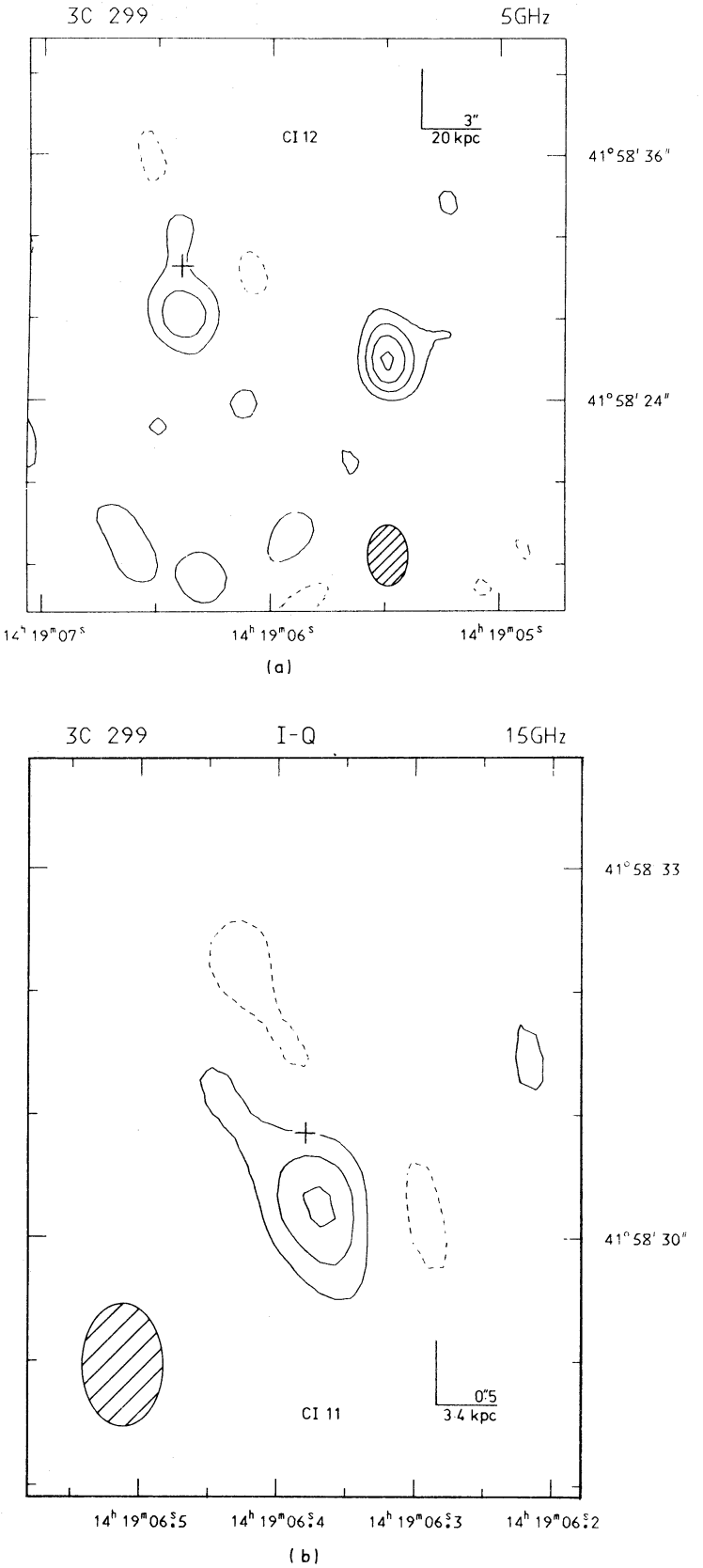

Figure 10. 3C 299. Both maps are phase-referenced. (a) 5.0 GHz. A point source of 0.90 Jy has been subtracted from the position marked by the cross. The lowest contour is 1.3 per cent of the peak. (b) 15.4 GHz. A point source of 0.18 Jy has been subtracted from the position marked by the cross. The lowest contour is 6.1 per cent of the peak.

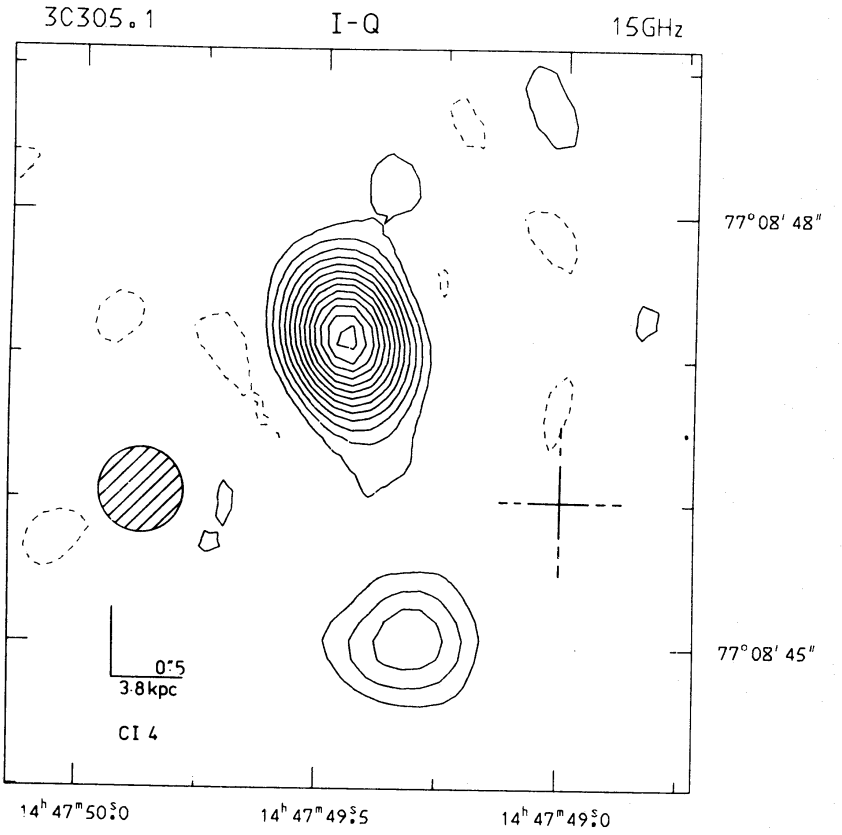

Figure 11. 3C 305.1 (not phase-referenced).

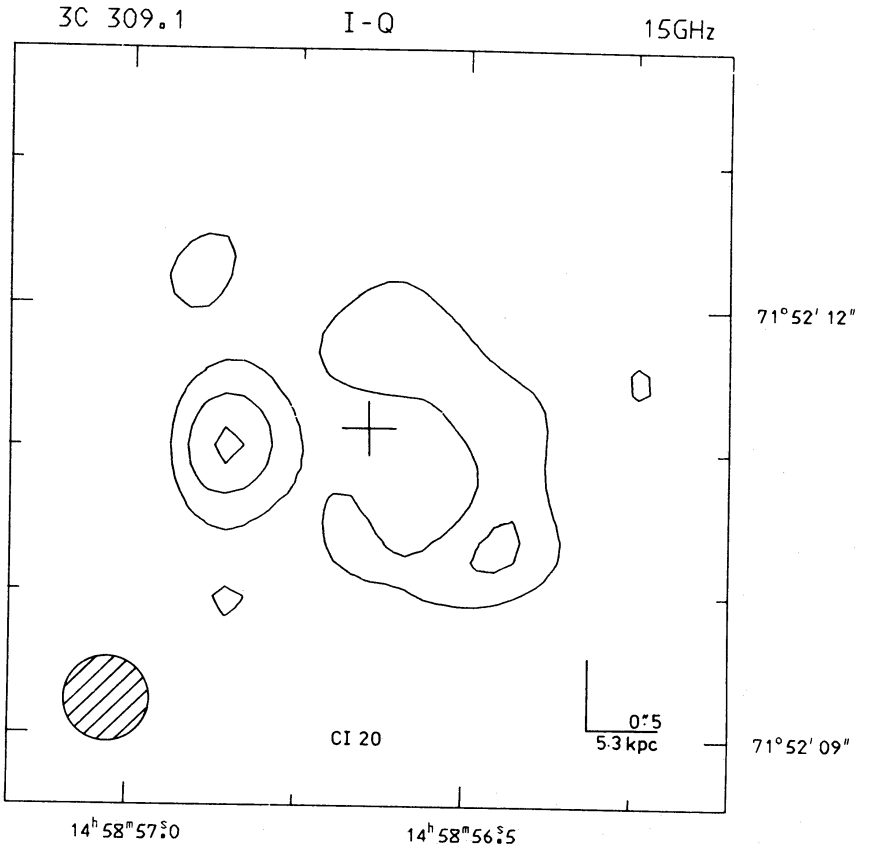

Figure 12. 3C 309.1 (phase-referenced). A point source of 0.99 Jy has been subtracted from the position marked by the closs. The lowest contour is 2.0 per cent of the peak.

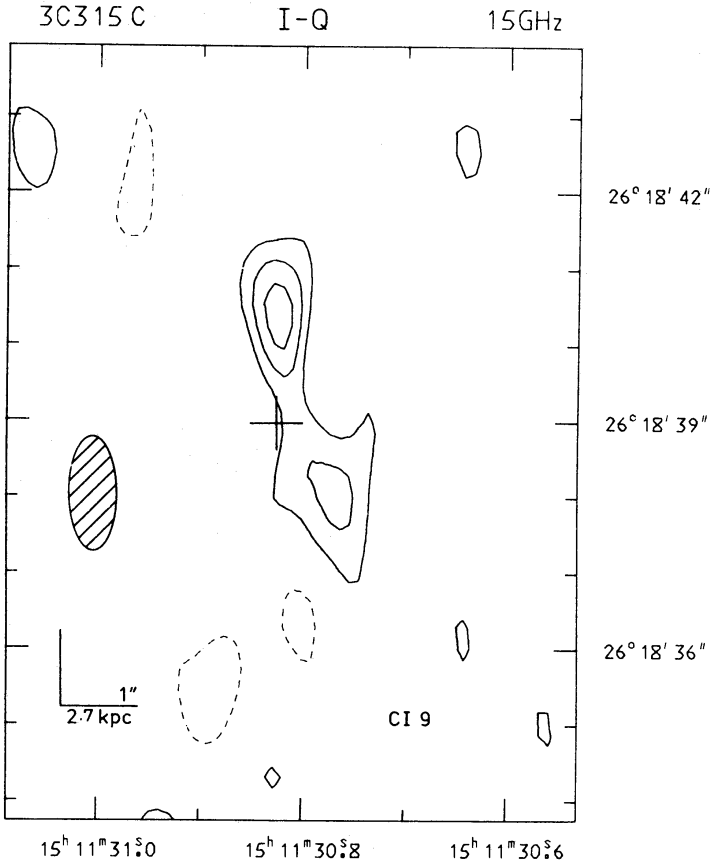

Figure 13. The central component of 3C 315 (not phase-referenced). The cross marks the position given by Griffin (1963) for the nucleus of the associated galaxy.

4.4 SOURCES IN WHICH THE OUTER STRUCTURE HAS NOT BEEN MAPPED

Details of these sources are given in Table 4, which lists their total flux densities and estimates or upper limits for the percentage of emission from resolved structure. The sources are divided into three categories:

(a) Phase-referenced and unresolved on the longest baseline. The residual structure (after subtraction of a point source from the map centre) is also given for these sources (see Section 3.2).

(b) Phase-referenced, but resolved.

(c) Not phase-referenced.

4.5 SPECTRA

For four of the resolved sources, the flux densities of central components have been measured at three or more frequencies. The spectra of compact cores and of extended structure can therefore be derived separately. The results are plotted in Fig. 16(a) to (d). It can be seen that the outer components have relatively steep spectra, as expected, but in two out of the four cases they show turnovers at low frequencies, which are presumably due to synchrotron self-absorption. The spectral indices and approximate turnover frequencies for the four sources are listed in Table 5. Results for 3C 345, 371 and 454.3 are also given.

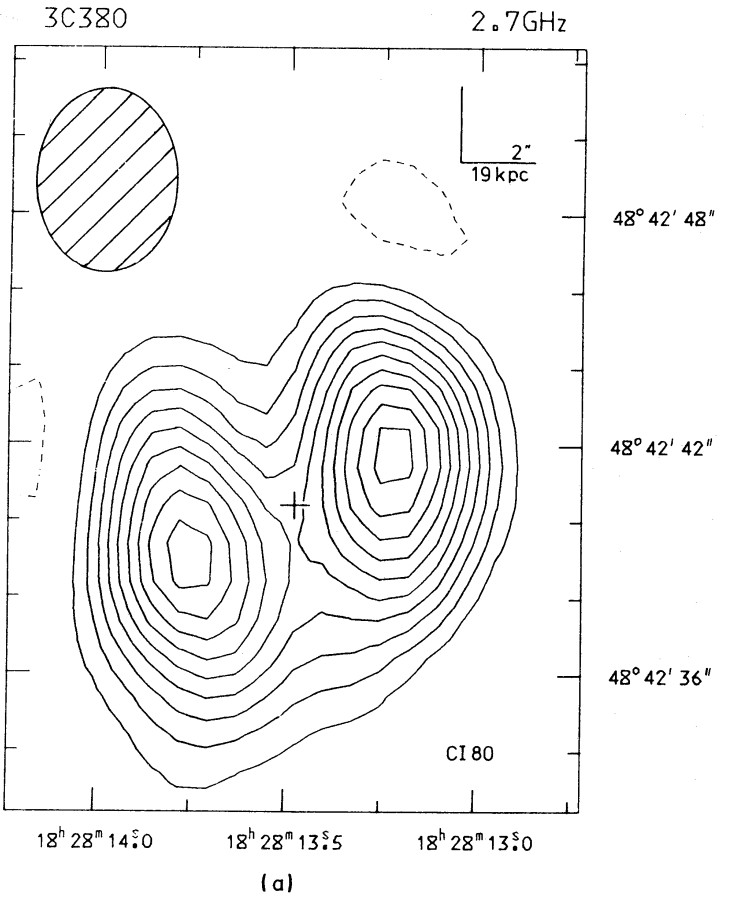

Figure 14. 3C 380. (a) 2.7 GHz (not phase-referenced). A point source of 6.16 Jy has been subtracted from the position marked by the cross. The lowest contour is 1.3 per cent of the peak.(b) 15.4 GHz (phase-referenced). A point source of 1.80 Jy has been subtracted from the position marked by the *lower* of the two crosses. The upper cross indicates the position of the second compact component described by Readhead & Wilkinson (1980; see Section 5). The contour level is 4.2 per cent of the peak. (c) A VLBI map of the core of 3C 380 at 1671 MHz, from Readhead & Wilkinson (1980). The restoring beam is a circular Gaussian of FWHM = 0.003 arcsec; the contours are plotted at 18, 54, 90,... 414×10^8 K.

5 Notes on the sources

3C43. Partially resolved in pa ~ 6°.

3C48. The brightness distribution of 3C 48 is dominated by a compact CC, and phase-referencing on this component shows that the outer structure is extended in pa ~ 7° and is separated from the core by ~ 0.8 arcsec.

3C49. Partially resolved.

3C138. This source is clearly resolved on the longest baselines at 15.4 GHz, but atmospheric phase errors were particularly bad because of its low declination. In addition, the results of Donaldson, Miley & Palmer (1971) show that there is structure in the core on a scale of 0.4 arcsec in pa 70°, which is too extended to allow reliable mapping of any outer components.

3C147. Phase-referencing on the CC of 3C 147 shows that the source has outer structure separated from the CC by ~ 0.6 arcsec in pa 26°. For the reasons discussed in Section 3.3,

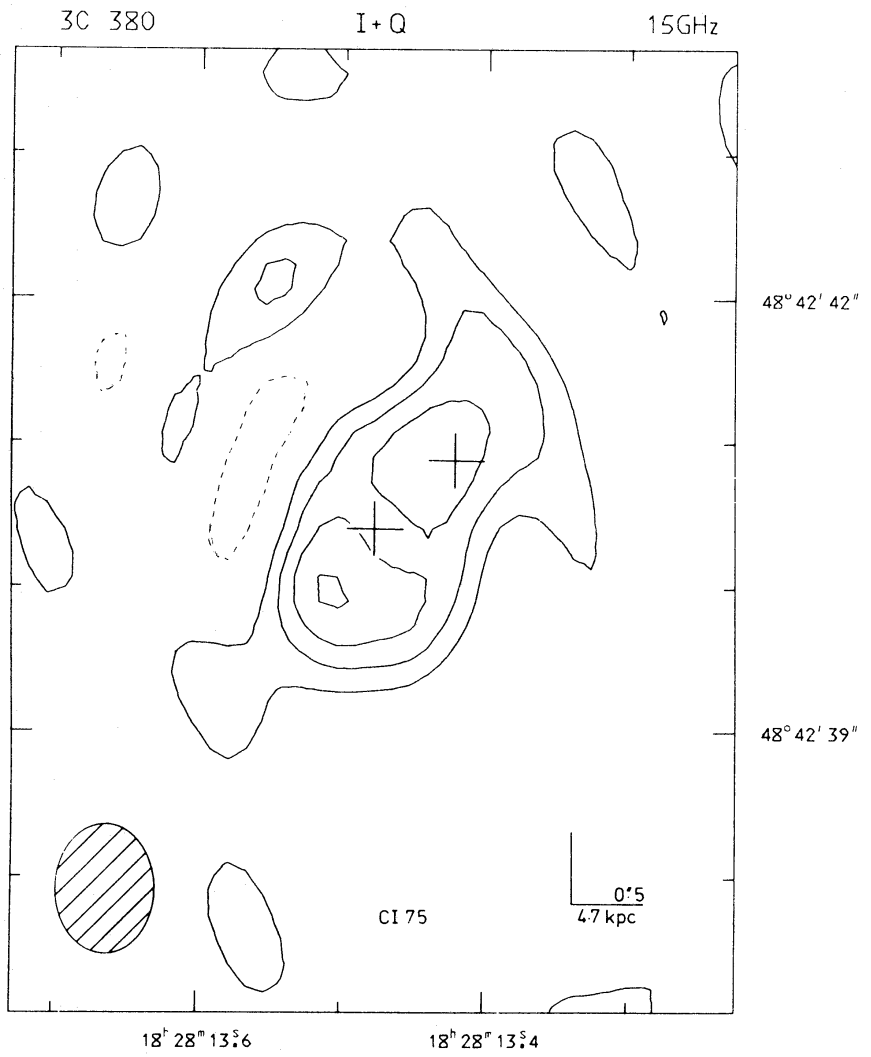

(b)

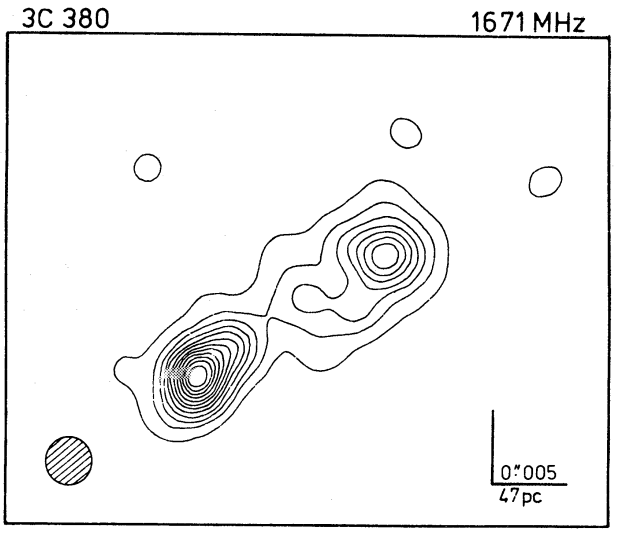

Figure 14(c)

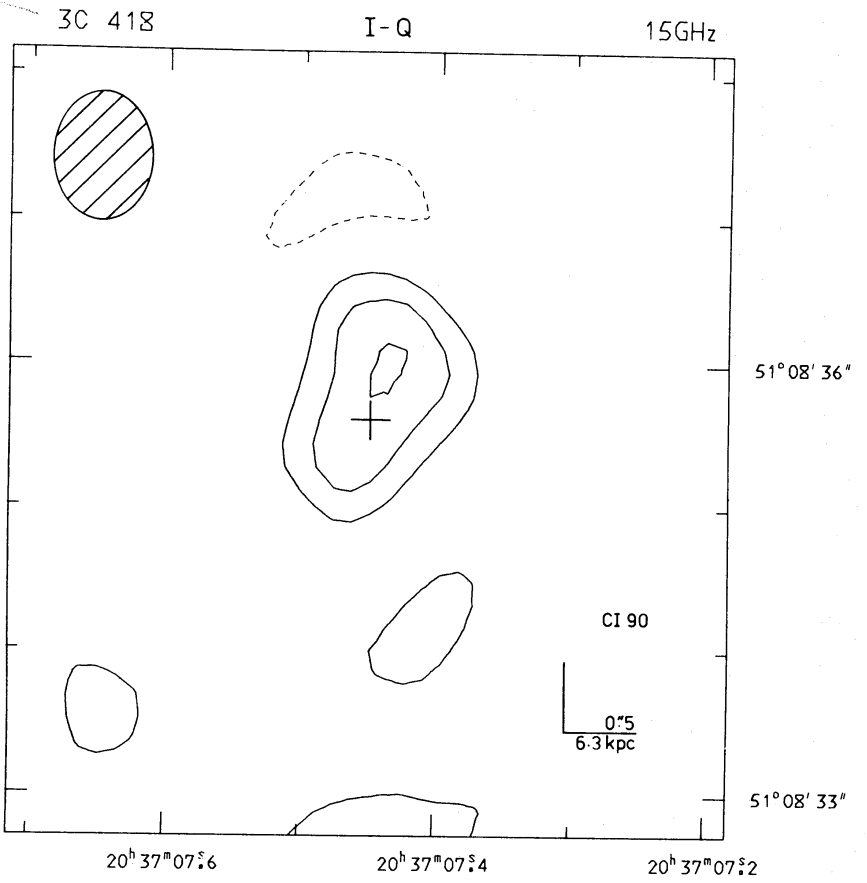

Figure 15. 3C418 (phase-referenced). A point source of 4.60 Jy has been subtracted from the position marked by the cross. The contour level is 2.0 per cent of the peak.

the presence of another component on the other side of the CC (i.e. in pa −154°) cannot be ruled out, but observations by Readhead, Napier & Bignell (1980) using the VLA at 4.9 and 15.0 GHz suggest that the outer structure is in fact one-sided. Their 15.0-GHz map reveals a component of angular size ~ 0.5 arcsec, separated from the core by ~ 0.4 arcsec in pa 25°. The positions derived for the outer component in both sets of synthesis observations and also in the single-baseline observations of Donaldson & Smith (1971) are in mutual agreement. The CC has been shown to have a core-jet structure of length 0.2 arcsec in pa 55° (Wilkinson et al. 1977; Readhead & Wilkinson 1980).

Readhead *et al.* (1978) have suggested that the misalignment between the inner and outer structures is due to the amplification of a slight (~ 5°) curvature by projection, the axis of the jet being at a small angle to the line-of-sight. It is interesting in this context that the outer component and jet of 3C 147 are on *opposite* sides of the nucleus (see Section 6). The morphology and physical size of the radio galaxy M87 (e.g. Laing 1980) are very similar, despite the large difference in luminosity. Both sources have compact central components, curved and irregular jets on one side, and extended emission which is more prominent on the side of the nucleus opposite the jet.

The approximate spectra of the various components of the source are shown in Fig. 16(a); the points are those given by Wilkinson *et al.* (1977) together with the present results at 15.4 GHz. The outer structure has a relatively steep spectrum with $\alpha = 1.23 \pm 0.06$ and a turnover at ~ 100 MHz. This should be compared with the value for the jet ($\alpha \sim 0.5$ between 609 and 1671 MHz, steepening to 0.7 at higher frequencies); the spectrum of the core is approximately flat between 500 and 3000 MHz, but must steepen at higher frequencies.

Table 3. Component parameters for resolved sources.

(a) Sources for which phase-referencing has been used

Source	Position RA(1950.0) h m s	Position Dec. (1950.0) ° ′ ″	Size/arcsec ω_1	ω_2	Flux density/mJy S	±	Flux density/mJy S	±	Total size Θ/arcsec	Position angle/degree
3C 245	10 40 05.648 ± 0.005	12 19 14.55 ± 0.33	< 0.5	< 2.5	40	10	850	90	4.9	90
	05.980	14.50 *			540	30				
3C 299	14 19 06.368 ± 0.006	41 58 30.25 ± 0.10	< 0.5	< 0.8	33	6	250	30	11.1	63
	06.380	30.90 *			180	20				
3C 309.1	14 58 56.644	71 52 11.15 *			990	50	1410	70	1.0	97
	56.858 ± 0.015	11.01 ± 0.07	< 0.3	< 0.3	65	7				
3C 380	18 28 13.478	48 42 40.40 *			1800	200	3400	300	-	143
	∼13.5	∼40	∼ 2.5	∼ 1.2	1600	200				
3C 418	20 37 07.45	51 08 35.60 *			4600	500	5300	500	1.5	156
	07.45 ± 0.02	36.0 ± 0.2	1.5	< 0.5	500	50				

(b) Sources for which phase-referencing has not been used

3C 190	07 58 44.96 ± 0.01	14 23 04.0 ± 0.4	< 0.4	< 1.6	40	10	250	30	2.4	-
	45.01 ± 0.01	22 58.2 ± 0.4	< 0.4	< 1.6	24	10				
	45.12 ± 0.01	23 04.6 ± 0.4	< 0.4	< 1.6	40	10				
3C 191	08 02 03.750 ± 0.014	10 23 59.1 ± 1.1	0.4	< 2	40	10	190	20	3.4	175
	03.770 ± 0.014	55.7 ± 1.1	0.4	< 2	50	10				
3C 236C	10 03 05.405 ± 0.006	35 08 47.90 ± 0.12	1.0	< 0.4	780	80	-	-	-	123.5
3C 268.3	12 03 54.067 ± 0.011	64 30 18.94 ± 0.08	< 0.3	< 0.3	150	20	300	30	1.3	61
	54.134 ± 0.011	17.49 ± 0.08	< 0.3	< 0.3	140	20				
3C 305.1	14 47 49.31 ± 0.02	77 08 45.03 ± 0.07	0.4	< 0.3	20	5	110	20	2.2	12
	49.45 ± 0.02	47.12 ± 0.07	0.5	< 0.2	70	7				
3C 315C	15 11 30.77 ± 0.01	26 18 38.0 ± 0.3	< 0.3	< 0.7	23	5	-	-	2.4	17
	30.82 ± 0.01	40.4 ± 0.3	< 0.3	< 0.7	32	6				

Table 4. Sources for which the outer structure is too weak to be mapped.

(a) Phase-referenced and unresolved

Source	Date of observation day/month/year	Flux density/mJy S	±	Residual structure after phase-referencing (per cent of peak) +	-
3C 93.1	16/1/76	290	20	3.5	3.5
4C 55.16	21/12/76	1710	100	3.6	0.6
	9/4/76			4.4	2.9
	16/1/77			2.1	1.4
OJ 287*	2/12/76	1900	100	4.4	2.9
	15/12/76	1750	100	4.3	5.8
	31/12/76	1780	100	7.0	7.2
	9/1/77	2100	100	2.3	5.3
	15/1/77	2330	100	3.0	5.0
3C 286	30/12/75	I = 3380 mJy		5.0	5.2
	31/3/76	(assumed value)		7.6	3.8
	5/1/77			5.1	6.0
2005+403	18/1/76	7100	400	3.8	1.9
CTA 102	10/11/76	2520	130	8.4	7.0
3C 454	12/2/77	310	20	3.0	6.1

* OJ 287 varied significantly during the observations; individual measurements are given.

(b) Phase-referenced and resolved

Source	Flux density / mJy S	±	Percentage of flux density in resolved component	Position angle / degree
3C 43	470	20	∿30	-
3C 48	1660	80	20	7
3C 49	310	20	∿30	-
3C 138	1650	80	30	-
3C 147	2780	140	12	26

(c) Not phase-referenced

3C 241	50	10	<20	-
3C 303.1	110	10	<20	-

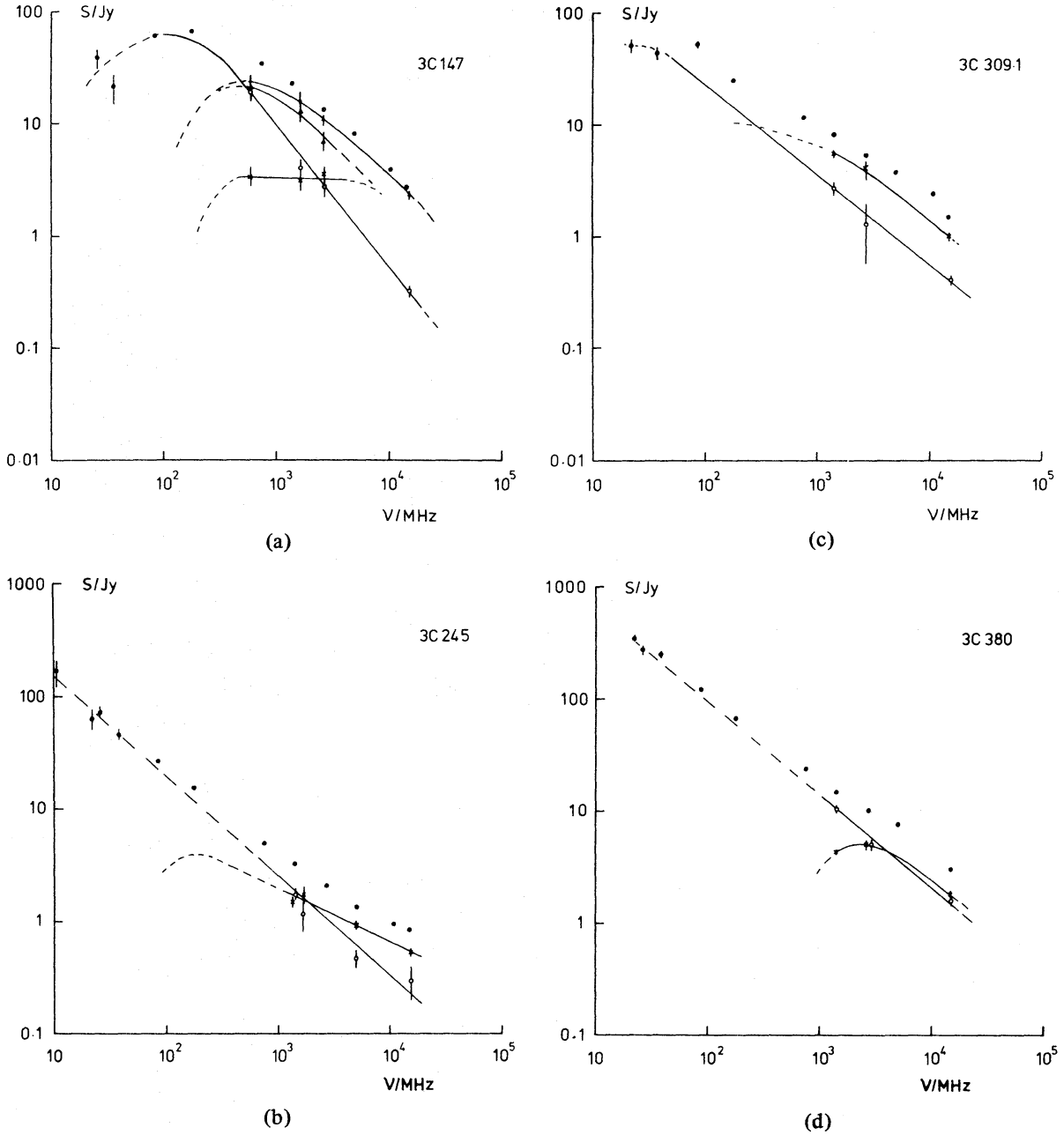

Figure 16. Spectra for the four sources which have reliable measurements at three or more frequencies of the flux densities due to the central components. ● Total flux density. × Flux density of the central component. + Flux density of the core and jet. ▲ Flux density of the jet. ○ Flux density of the extended structure. + and ▲ for 3C 147 only.

References for component flux densities:

ν(MHz)	Reference
15375	This paper
4995	This paper
2694	Donaldson & Smith (1971) as reanalysed by Wilkinson *et al.* (1977), Donaldson *et al.* (1969).
1660	Fort (1970), quoted by Wilkinson *et al.* (1977), Kellermann *et al.* (1971),
1422	Donaldson, Miley, Palmer & Smith (1969),
1417	Kapahi & Schilizzi (1979),
609	Wilkinson *et al.* (1977),

The flux-density scales used are those given by Baars *et al.* (1977) and by Laing & Peacock (1980).

Table 5. Spectra of extended structure around compact radio sources.

Source	Spectral index of extended structure α	±	Self-absorption turnover frequency ν_{SSA}/MHz	Reference
3C 147	1.23	0.06	∼100	1
3C 245	0.90	0.20	< 10	1
3C 309.1	0.80	0.04	∼ 20	1
3C 380	0.81	0.11	< 20	1
3C 345	1.00	0.05	< 20	2
3C 371	1.15	0.10	< 40	2
3C 454.3	1.00	0.10	∼ 60 ?	3

References : 1 This paper,
2 Perley & Johnston (1979),
3 Davis, Stannard & Conway (1977).

3C190. There is no dominant component in 3C 190 at 15.4 GHz, so that phase-referencing has not been attempted. The map is therefore disfigured by the effects of tropospheric phase irregularities. The source has three components (Fig. 4; the feature at Dec 14° 23′ 14″ is weak and may not be real). It is not clear whether the associated quasar, whose position is marked by the cross in Fig. 4, is coincident with either of the brighter components; a better radio map and a more accurate optical position are needed.

3C191. This source is resolved into a double with a separation of 3 arcsec in pa −5°; a map made using a uniform grading of the aperture is shown in Fig. 5. The details of the structure are uncertain because of the low resolution in declination.

4C55.16. This source is unresolved in the present observations; the maximum compact structure after removal of the central component is ∼ 4 per cent of the peak. Wilkinson (1972) suggested tentatively that ∼ 14 per cent of the emission at 1423 MHz comes from a region of size ∼ 3 arcsec.

0J287. The optical identification of 0J 287 is a highly-variable BL Lac object; the source is unresolved at 15.4 GHz. There is evidence for flux-density variations over the 6-week period over which the observations were made (Table 4).

3C236. The map of Fig. 6(a) shows only the CC of this huge triple source (Willis, Strom & Wilson 1974). The CC has previously been mapped by Fomalont & Miley (1975), while more detailed studies have been presented by Fomalont, Miley & Bridle (1979) and by Schilizzi *et al.* (1979). The position angle determined in the present observations (123°.5 ± 1°) is in good agreement with thatof the extended structure (122°.5 ± 2°). Schilizzi *et al.* (1979) have shown that the structure of the CC is complex, with at least five components. Their model brightness distribution is shown in Fig. 6(b) (note that observations of closure phase have been used to resolve the 180° ambiguity in orientation). The location of the flat-spectrum nuclear component detected by Preuss *et al.* (1977) is not certain, but it would seem most likely that it is component B2 of Fig. 6(b). Our present knowledge of the structure of the CC of 3C 236 may be summarized as follows:

(1) the overall length is ∼ 1 arcsec (2.5 kpc);

(2) there is structure on scales ranging from ∼ 0.001 arcsec (2.5 pc) to ∼ 0.6 arcsec (1.5 kpc);

(3) the brightness distribution is very asymmetrical;

(4) the 1-arcsec structure is aligned with the outer components, as are the bright features B1 and B2; the components A and C are offset from this axis;

(5) the spectral index has a remarkably uniform value of 0.5 across the CC between 0.4 and 22.5 GHz;

(6) The 0.001-arcsec component is most likely to be located in B2.

3C241. This source is unresolved at 15.4 GHz and is too weak for phase-referencing.

3C245. Jenkins *et al.* (1977) described observations of 3C 245 at 5.0 GHz with the 5-km telescope; a re-analysis of their data using the brighter component as a phase reference gives the map shown in Fig. 7(a). The source consists of at least three components as follows:

(a) A compact CC, coincident with the associated quasar, which has been subtracted from the map to show the extended structure; its position is marked by a cross.

(b) An unresolved component 4.6 arcsec away from the CC in pa $-83°$.

(c) A weaker component 2.5 arcsec to the east of the CC.

The positions and flux densities of these features at 5.0 GHz are as follows:

RA (1950.0) h	m	s	Dec (1950.0) °	′	″	Flux density (mJy) S	±
10	40	05.67 ± 0.02	12	19	15.1 ± 1.4	200	20
⋆		05.98			14.5	910	90
		06.15 ± 0.02			13.9 ± 1.4	100	50

(⋆ assumed position for phase reference).

3C 245 has also been observed at 15.4 GHz (Fig. 7b). At this frequency, only the two brighter components are detected; both are unresolved. The source is therefore very asymmetrical, but there is emission on *both* sides of the nucleus. Lyne (1972) observed lunar occultations of 3C 245 at 240, 408 and 1420 MHz. His conclusions were as follows:

(a) The preceding component is resolved along the source axis with $\theta \sim 3$ arcsec at 408 MHz. There is therefore likely to be some extended emission between the CC and the hot-spot of the preceding component which is not detected at 5.0 GHz.

(b) There is an extended component 2 arcsec to the east of the CC with $\theta \sim 2$ arcsec (compare Fig. 7a).

The present observations suggest the 3C 245 is a triple source whose outer components have flux densities in the ratio 2:1 at 5 GHz. Spectra are plotted separately for the CC and for the extended structure in Fig. 16(b). The extended structure has $\alpha \sim 0.9$.

3C268.3. This source is resolved into a double of separation 1.3 arcsec with roughly equal component intensities (Fig. 8). The identification suggested by Kristian, Sandage & Katem (1974) is a galaxy in a rich cluster; its position is, however, significantly displaced from the source axis. A more accurate optical position is needed to establish whether or not the identification is correct. The model derived for 3C 268.3 by Wilkinson (1972) from single-baseline observations at 1423 MHz gives a component separation and position angle (1.3 arcsec in pa 163°) which agree well with the results derived at 15.4 GHz, but the flux densities of the two components are 2.2 Jy and 0.9 Jy, implying spectral indices of ~ 1.1 and ~ 0.8, respectively.

3C 286. This source is unresolved at 15.4 GHz, with less than 5 per cent of its flux density coming from extended structure, and is used as the primary calibrator at this frequency. The VLBI observations by Wilkinson *et al.* (1979) at 609 MHz reveal a structure consisting of a compact region (10 × 5 milliarcsec in pa 42°) with a jet-like component whose angular extent is 40 × 15 m.arcsec in pa 42° (Fig. 9). The jet bends to a position angle of 30° ± 5° at a distance of ~ 0.02 arcsec from the core. The core and jet dominate the emission from 3C 286 for $\nu \gtrsim 1400$ MHz. At such frequencies, the source is highly polarized (9 per cent at 1.4 GHz, rising to 12 per cent at 10 GHz) and the rotation measure is small and accurately defined. The decomposition of the spectrum of 3C 286 given by Wilkinson *et al.* (1979) and the high percentage polarization both indicate that most of the emission comes from regions which are optically thin. The direction of the magnetic field has been inferred from a fit to the position angle of the integrated linear polarization between 1.4 and 10.7 GHz on this assumption. The position angle of the apparent magnetic field is 122°.6 ± 0°.4 ($\chi^2 = 12.9$ with 15 degrees of freedom). As can be seen from Fig. 9, this is almost perpendicular to the axis of the outer jet. In this respect, 3C 286 resembles low-luminosity radio galaxies such as 3C 31 (Burch 1979), which also has jets in which the apparent magnetic field is perpendicular to the axes. The only other core-jet structures on scales of 10^{-2} arcsec with known field directions are those in 3C 273, 345 and 454.3, for which Davis, Stannard & Conway (1978) inferred field directions *parallel* to their axes.

3C 299. Riley & Pooley (1975) suggested that 3C 299 might have a D2 morphology, with a bright, compact component coincident with the associated 19-mag double galaxy and possibly a faint component 11 arcsec to the south-west. The latter feature is confirmed by a re-analysis of the 5-GHz data using phase-referencing (Fig. 10a). There may also be a weak extension to the south of the bright component. There is no compact structure brighter than 20 mJy to the east of the galaxy. The parameters of the components observed at 5.0 GHz are as follows:

RA (1950.0) h	m	s	Dec (1950.0) °	′	″	Flux density (mJy) S	±
14	19	05.49 ± 0.02	41	58	25.9 ± 0.3	48	10
⋆		06.38			30.9	900	90
		06.39 ± 0.02			28.1 ± 0.3	35	10

(⋆ assumed position for phase reference).

The 15.4-GHz observations were not sensitive enough to reveal the preceding component: a map of the region around the bright component is shown in Fig. 10. An extension to the south of the bright component is also visible on this map. The morphology of this source is puzzling; it has some similarities with that of 3C 293 (Argue, Riley & Pooley 1978) which also has two components close to the identification and a third one much farther away. There is no doubt in the case of 3C 293 that the components are physically related, but the source is much less luminous than is 3C 299. Three possible explanations for the structure of 3C 299 are:

(a) The preceding component is unrelated to the rest of the source.

(b) There is another component to the north-east of the galaxy which has remained undetected in the present observation.

(c) The identification is incorrect and (for example) one of the other galaxies in the surrounding cluster is associated with the radio source. Support for this explanation comes from the fact that the spectrum of the brighter component is steep ($\alpha \sim 1.1$).

More sensitive radio observations are needed to search for a component to the north-east of the galaxy, for a bridge of emission joining the two brighter components and for a CC between them. Deeper optical pictures would also be valuable.

3C303.1. This source is unresolved at 15.4 GHz and is too weak for phase referencing.

3C305.1. The 15.4-GHz map of Fig. 11 shows this source to be double. The northern and southern components are resolved parallel (pa 16°) and perpendicular (pa 102°) to the source axis respectively. The optical position of the associated galaxy (Kristian *et al.* 1974) is insufficiently precise to determine whether the source has classical-double or D2 morphology. The former alternative seems more likely because both components are extended and the high-frequency spectrum is steep.

3C309.1. The phase-referenced map of Fig. 12 shows that there are two compact components in this source, separated by 1.0 arcsec in pa 97° with flux densities of 990 and 65 mJy. Twenty-five per cent of the flux density of the source is in resolved structure whose location is uncertain (there may be some extended emission to the west of the brighter component). The spectral index of the brighter component between 1.4 and 15.4 GHz, $\alpha = 0.72 \pm 0.04$, is very similar to that of the rest of the source, $\alpha = 0.80 \pm 0.04$ (Fig. 16c). It may therefore be that the bright component is not a central core coincident with the associated quasar. Better absolute measurements of component positions are needed to settle this point.

3C315. The 15.4-GHz observations refer only to the CC of this peculiar source (Högbom 1979); the map of Fig. 13 shows that the CC is resolved into two components separated by 2.4 arcsec in pa 17° on either side of the associated galaxy (Griffin 1963). The position angle agrees with that of the extended structure close to the nucleus, and may indicate the beginning of a jet.

3C380. 3C 380 is partially resolved by the 5-km telescope at 2.7 GHz; there is extended structure in pa ~ 117° on both sides of the nucleus (Fig. 14a). A reanalysis of the 5.0-GHz data of Jenkins *et al.* (1977), using phase-referencing, shows the following features:

(a) There is collimated structure in pa 128° within ~ 4 arcsec of the nucleus. For the reasons discussed in Section 3.3, it is uncertain whether this emission is located on one or both sides of the nucleus.

(b) A halo of low surface brightness extends to the north of the nucleus; its dimensions are ~ 8 and ~ 4 arcsec respectively in RA and in Dec.

A 15.4-GHz map of the inner region of the source is presented in Fig. 14(b) which shows that the emission around the nucleus is extended asymmetrically in pa −38°. It is possible that the collimated emission seen at 5.0 GHz is also one-sided, but the derived position angle for the structure on this scale would then be −52°.

3C 380 has also been observed using VLBI at 1671 MHz by Readhead & Wilkinson (1980); their map of the central region is shown in Fig. 14(c). They suggest that the south-east component is the core of the object and is responsible for its variability (e.g. Medd *et al.* 1972). The VLBI structure is orientated in pa −58°. Readhead & Wilkinson also detected another component with $\theta < 0.1$ arcsec at a distance of 0.7 arcsec from the core; this is marked by the upper cross in Fig. 14(b).

It is difficult to separate the integrated spectrum of 3C 380 into components because of the complicated structure of the source; a tentative decomposition into core (< 0.2 arcsec) and extended structure is shown in Fig. 16(d). The core has a turnover frequency of

~ 2.5 GHz and the extended structure has $\alpha = 0.81 \pm 0.11$; an extrapolation of the latter gives a reasonable fit to the spectrum at low frequencies.

2005+403. Unresolved.

3C418. This source has been observed by Perley & Johnston (1979) with the VLA at 1.5 and 4.9 GHz. They suggested that the source is of the D2 type (Miley 1971) with a component separation of 1.6 arcsec in pa 146°, but were unable to make a map. The 15.4-GHz map of Fig. 15 confirms this result, but gives a pa of 156° ± 4°.

CTA 102. Unresolved.

3C454. Unresolved.

6 Discussion

In this paper, observations of 25 (predominantly compact) radio sources have been presented. Their structures can be classified as follows:

(1) Double, without a central component: 3C 191, 268.3 and 305.1.

(2) Nucleus of a radio galaxy (extended in the same direction as the large-scale emission): 3C 236 and 315.

(3) Bright central core, with weak outer structure: 3C 48, 138, 147, 245, 309.1, 380 and 418.

(4) Well-resolved, but relationship to optical identification uncertain: 3C 190 and 299.

(5) Unresolved: 3C 43, 49, 93.1, 241, 286, 303.1, 454, 4C 55.16, 0J 287, 2005 + 403 and CTA 102.

The sources listed in (3) above are particularly interesting because their cores can be mapped using VLBI, and structure on scales ranging from 10^{-3}–10 arcsec can be compared. There are two pieces of evidence which suggest that emission on a scale of ~ 1 arcsec is present in all such objects selected at a low frequency.

(a) The compact cores which dominate the emission at high frequencies are expected to be self-absorbed at 178 MHz (see, e.g. the spectra given in Fig. 16).

(b) Measurements of interplanetary scintillation at 81.5 MHz suggest that all the sources have $\theta \gtrsim 0.4$ arcsec (Duffett-Smith 1980). In contrast, sources selected in high-frequency surveys (e.g. 0J 287) tend to have very little emission at frequencies below 500 MHz, suggesting that outer structure is weak or absent.

Eight sources in a complete sample of 41 spectroscopically-confirmed quasars selected at 178 MHz (the quasars from the sample defined by Jenkins *et al.* 1977) have CCs which contribute more than half of their flux densities at 5.0 GHz, together with detectable outer structure (Davis *et al.* 1977; Perley & Johnston 1979, and the present paper). They are: 3C 48, 138, 147, 245, 309.1, 345, 380 and 454.3. At least three other objects in the sample (3C 216, 286 and 287) have bright CCs and, for the reasons given earlier, are also likely to have extended structure. There are thus at least 11 examples of this class of source in a sample of 41 bright quasars selected at 178 MHz.

A natural explanation for the structures of the compact radio sources is provided by the relativistic jet model of Scheuer & Readhead (1979), in which both compact and extended radio sources are supposed to be produced by twin beams with relativistic bulk velocity, whose radiation is strongly beamed. Outer components correspond to the points of impact

of the beams on the intergalactic medium. If the source axis makes a small angle ($\lesssim 1/\gamma$, where γ is the Lorentz factor of the flow) with the line-of-sight, then:

(1) The CC will be bright, with a one-sided structure, because radiation from the nearer jet will be beamed towards us.

(2) Any curvature intrinsic to the jet will be amplified by projection effects, so that there may be large misalignments between structure on different scales.

(3) The outer components will appear projected against the core. Within the framework of this model, two possibilities for the morphology of the outer structure have been discussed, as follows:

(a) Scheuer & Readhead (1979) suggested that the *outer* structure in the quasars which show apparent superluminal expansion (3C 273, 345 and 454.3) is moving relativistically. Such emission is then expected to be visible only on the same side of the nucleus as the VLBI jet, as observed. Sources whose axes are close to the line-of-sight would then be selected preferentially even in a low-frequency survey.

(b) In other compact objects, it may be that the outer components have velocities typical of hot-spots in extended doubles ($v \sim 0.05c$; Readhead 1980) and therefore radiate isotropically, implying that the orientations of sources selected in a low-frequency survey will be randomly distributed. Sources which have outer structure on the opposite side of the nucleus to the VLBI jet (e.g. 3C 147) or on both sides of the nucleus (e.g. 3C 245) may fall into this category.

Further synthesis observations (preferably of a complete sample) are required to determine whether the majority of core sources have one-sided outer structure and consequently whether sources whose axes are close to the line-of-sight might be selected preferentially in a low-frequency survey. VLBI mapping of the core sources which have been resolved in the present observations would also be valuable.

Acknowledgments

I am grateful to Tony Readhead for stimulating my interest in this subject and for permission to reproduce maps of 3C 286 and 3C 380. I also thank Dr R. T. Schilizzi and his colleagues for allowing me to reproduce Fig. 6(b), Dr P. N. Wilkinson for a critical review of the manuscript and John Baldwin, Guy Pooley, Peter Scheuer, John Shakeshaft and Peter Warner for their help and advice. I acknowledge financial support from the SRC and the Cavendish Laboratory.

References

Argue, A. N. & Kenworthy, C. M., 1972. *Mon. Not. R. astr. Soc.*, **160**, 197.

Argue, A. N., Clements, E. D., Harvey, G. M. & Murray, C. A., 1978. *Modern astrometry, IAU Coll. 48*, p. 155, eds Prochazka, F. V. & Tucker, R. H., Institute of Astronomy, Vienna.

Argue, A. N., Riley, J. M. & Pooley, G. G., 1978. *Observatory*, **98**, 192.

Baars, J. W. M., Genzel, R., Pauliny-Toth, I. I. K. & Witzel, A., 1977. *Astr. Astrophys.*, **61**, 99.

Boksenberg, A., Briggs, S. A., Carswell, R. F., Schmidt, M. & Walsh, D., 1976. *Mon. Not. R. astr. Soc.*, **177**, 43P.

Bracewell, R. N. & Thompson, A. R., 1973. *Astrophys. J.*, **182**, 77.

Burbidge, G. R. & Crowne, A. H., 1979. *Astrophys. J. Suppl. Series*, **40**, 583.

Burch, S. F., 1979. *Mon. Not. R. astr. Soc.*, **187**, 187.

Davis, R. J., Stannard, D. & Conway, R. G., 1977. *Nature*, **267**, 596.

Davis, R. J., Stannard, D. & Conway, R. G., 1978. *Mon. Not. R. astr. Soc.*, **185**, 435.

de Vegt, Chr. & Gehlich, U. K., 1978. *Modern astrometry, IAU Coll. 48,* p. 113, eds Prochazka, F. V. & Tucker, R. H., Institute of Astronomy, Vienna.
Donaldson, W. & Smith, H., 1971. *Mon. Not. R. astr. Soc.,* **151**, *253.*
Donaldson, W., Miley, G. K., Palmer, H. P. & Smith, H., 1969. *Mon. Not. R. astr. Soc.,* **146**, 213.
Duffett-Smith, P. J., 1980. *Mon. Not. R. astr. Soc.,* **192**, 33.
Fomalont, E. B. & Miley, G. K., 1975. *Nature,* **257**, 99.
Fomalont, E. B., Miley, G. K. & Bridle, A. H., 1979. *Astr. Astrophys.,* **76**, 106.
Genzel, R., Pauliny-Toth, I. I. K., Preuss, E. & Witzel, A., 1976. *Astr. J.,* **81**, 1084.
Griffin, R. F., 1963. *Astr. J.,* **68**, 421.
Hamaker, J. P., 1979a. *Image formation from spatial coherence functions in astronomy, IAU Coll. 49,* p. 27, ed. van Schooneveld, C., D. Reidel, Dordrecht, Holland.
Hamaker, J. P., 1979b. *Ibid,* p. 47.
Hargrave, P. J., & Shaw, L. J., 1978. *Mon. Not. R. astr. Soc.,* **182**, 233.
Högbom, J. A., 1979. *Astr. Astrophys., Suppl.,* **36**, 173.
Jenkins, C. J., Pooley, G. G. & Riley, J. M., 1977. *Mem. R. astr. Soc.,* **84**, 61.
Kapahi, V. K. & Schilizzi, R. T., 1979. *Astr. Astrophys. Suppl.,* **38**, 11.
Kellermann, K. I., Jauncey, D. L., Cohen, M. H., Shaffer, B. B., Clark, B. G., Broderick, J., Rönnäng, B., Rydbeck, O. E. H., Matveyenko, I., Vitkevich, V. V., Cooper, B. F. C. & Batchelor, R., 1971. *Astrophys. J.,* **169**, 1.
Kinman, T. D., 1976. *Astrophys. J.,* **205**, 1.
Kristian, J., Sandage, A. & Katem, B., 1974. *Astrophys. J.,* **191**, 43.
Kristian, J., Sandage, A. & Katem, B., 1978. *Astrophys. J.,* **219**, 803.
Laing, R. A., 1980. *Mon. Not. R. astr. Soc.,* **193**, 427.
Laing, R. A. & Peacock, J. A., 1980. *Mon. Not. R. astr. Soc.,* **190**, 903.
Laing, R. A., Longair, M. S., Riley, J. M., Kibblewhite, E. J. & Gunn, J. E., 1978. *Mon. Not. R. astr. Soc.,* **183**, 547.
Lyne, A. G., 1972. *Mon. Not. R. astr. Soc.,* **158**, 431.
Medd, W. J., Andrew, B. H., Harvey, G. A. & Locke, J. L., 1972. *Mem. R. astr. Soc.,* 77, 109.
Miley, G. K., 1971. *Mon. Not. R. astr. Soc.,* **152**, 477.
Peckham, R. J., 1973. *Mon. Not. R. astr. Soc.,* **165**, 25.
Perley, R. A. & Johnston, K. J., 1979. *Astr. J.,* **84**, 1247.
Preuss, E., Pauliny-Toth, I. I. K., Witzel, A., Kellermann, K. I. & Shaffer, D. E., 1977. *Astr. Astrophys.,* **54**, 297.
Readhead, A. C. S., 1980. *Objects of High Redshift, IAU Symp. 92,* p. 165, eds Abell, G. O. & Peebles, P. J. E., D. Reidel, Dordrecht, Holland.
Readhead, A. C. S. & Hewish, A., 1974. *Mem. R. astr. Soc.,* 78, 1.
Readhead, A. C. S. & Wilkinson, P. N., 1978. *Astrophys. J.,* **223**, 25.
Readhead, A. C. S. & Wilkinson, P. N., 1980. *Astrophys. J.,* **235**, 11.
Readhead, A. C. S., Cohen, M. H., Pearson, T. J. & Wilkinson, P. N., 1978. *Nature,* **276**, 768.
Readhead, A. C. S., Napier, P. J. & Bignell, R. C., 1980. *Astrophys. J.,* **237**, L55.
Riley, J. M., Longair, M. S. & Gunn, J. E., 1980. *Mon. Not. R. astr. Soc.,* **192**, 233.
Riley, J. M. & Pooley, G. G., 1975. *Mem. R. astr. Soc.,* **80**, 105.
Riley, J. M. & Pooley, G. G., 1978. *Mon. Not. R. astr. Soc.,* **183**, 245.
Scheuer, P. A. G. & Readhead, A. C. S., 1979. *Nature,* **277**, 182.
Schilizzi, R. T., Miley, G. K., van Ardenne, A., Baud, B., Bååth, L., Rönnäng, B. O. & Pauliny-Toth, I. I. K., 1979. *Astr. Astrophys.,* 77, 1.
Schmidt, M., 1965. *Astrophys. J.,* **141**, 1295.
Smith, H. E., Spinrad, H. & Smith, E. O., 1976. *Publs astr. Soc. Pacif.,* 88, 621.
Tabara, H. & Inoue, M., 1980. *Astr. Astrophys. Suppl.,* 39, 379.
Wade, R. W., Hoessel, J. G., Elias, J. H. & Huchra, J. P., 1979. *Publs astr. Soc. Pacif.,* **91**, 35.
Wilkinson, P. N., 1972. *Mon. Not. R. astr. Soc.,* **160**, 305.
Wilkinson, P. N., Readhead, A. C. S., Purcell, G. H. & Anderson, B., 1977. *Nature,* **269**, 764.
Wilkinson, P. N., Readhead, A. C. S., Anderson, B. & Purcell, G. H., 1979. *Astrophys. J.,* **232**, 365.
Willis, A. G., Strom, R. G. & Wilson, A. S., 1974. *Nature,* **250**, 625.
Wills, B. J., Wills, D. & Douglas, J. N., 1973. *Astr. J.,* 78, 521.